Microporous and Mesoporous Materials 310 (2021) 110594

Contents lists available at ScienceDirect

Microporous and Mesoporous Materials

journal homepage: http://www.elsevier.com/locate/micromeso

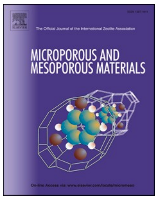

Noble metal location in porous supports determined by reaction with phosphines

C. Rieg [a], D. Dittmann [a], Z. Li [a], A. Kurtz [a], I. Lorenz [a], D.P. Estes [a], M. Buchmeiser [b], M. Dyballa [a,*], M. Hunger [a]

[a] Institute of Chemical Technology, University of Stuttgart, 70569, Stuttgart, Germany
[b] Institute of Polymer Chemistry, University of Stuttgart, 70569, Stuttgart, Germany

ARTICLE INFO

Keywords:
Mesoporous supports
Zeolite Y
Noble metal distribution
Triphenylphosphine
Tris(4-methoxyphenyl)phosphine
Solid-state NMR spectroscopy

ABSTRACT

Different phosphines (PR_3, R = phenyl, 4-methoxyphenyl) are demonstrated to be useful probe molecules for the spatial location and quantification of noble metal (NM) atoms within mesoporous and microporous support materials, such as silica A200, mesoporous SBA-15, and different zeolites Y. For this purpose, the high NMR sensitivity of ^{31}P nuclei (spin $I = ½$, abundance of 100%) and the characteristic chemical shifts of phosphine complexes formed with noble metals were utilized. A straightforward method of physically mixing the reduced noble metal-containing catalysts with the solid phosphine powders and heating under well-defined conditions is shown. Complexation of triphenylphosphine (PPh_3) and tris(4-methoxyphenyl)phosphine, $P(PhOMe)_3$, with Pt, Rh, Pd, and Ru on open surfaces and in mesopores leads to characteristic ^{31}P MAS NMR signals at $\delta = 33–41$ ppm. Because of the different molecular diameters of PPh_3 (0.72 nm) and $P(PhOMe)_3$ (0.91 nm), adsorption of these two probe molecules allows to distinguish between noble metal atoms located at the outer surface of zeolite particles and those in secondary mesopores and in supercages of zeolites Y. For the first time this method enables the characterization of noble metals directly using probe molecules and ^{31}P MAS NMR spectroscopy.

1. Introduction

The location of catalytically active sites in porous solids has a significant influence on the catalytic activity of these materials in chemical processes. Therefore, the investigation of the spatial distribution of the active centers is an important task for developing an in-depth understanding of shape-selective heterogeneous catalysts. For characterizing the properties and location of Brønsted and Lewis acid sites in pores and cages of solid catalysts, probe molecules with different basicity and molecule sizes, such as ammonia, pyridine, acetonitrile, and trimethylphosphine oxide, have been utilized [1–5]. In a similar manner, the knowledge of the location of metal particles, responsible for the hydrogenation and dehydrogenation properties of porous catalysts, helps to gain deeper insights into the reasons of their shape-selective properties [6–8].

Analytical techniques for clarifying the location of metal atoms in well-ordered crystalline support materials are often based on diffraction methods [9,10], while an insight into the local structure, also of less-ordered metal-containing catalysts, is possible by X-ray absorption methods [11,12]. Both techniques were demonstrated to be very useful for determining the distribution and coordination of metal sites in a large variety of solid catalysts, but are time-consuming and often not accessible. They also require long measurement times or high X-ray fluxes to receive diffractograms or absorption spectra of sufficient accuracy for simulation. Even if the location of the noble metal sites is known, the accessibility for adsorbates stays unclear.

Solid state NMR studies can give indirect insights into the location of noble metals (NM) [13,14]. Recently, triphenylphosphine (PPh_3) was demonstrated to be a useful probe molecule for the investigation of the accessibility of noble metals platinum (Pt) and rhodium (Rh) on mesoporous and microporous support materials [15]. The complex formation of PPh_3 with these noble metal species was identified by the occurrence of downfield shifted ^{31}P MAS NMR signals at characteristic isotropic chemical shifts and chemical shift anisotropies [15]. Based on this study, the present work has the aim of increasing the variety of noble metal species by palladium (Pd) and ruthenium (Ru) for the study of their complexation with phosphines and to investigate the effect of framework aluminum in zeolites Y on the location of these species.

---

* Corresponding author.
E-mail address: michael.dyballa@itc.uni-stuttgart.de (M. Dyballa).

https://doi.org/10.1016/j.micromeso.2020.110594
Received 8 June 2020; Received in revised form 3 August 2020; Accepted 27 August 2020

Furthermore, phosphines with different sizes were applied for deeper insights into the spatial location of noble metal sites, especially in the case of microporous support materials.

For a proper choice of suitable probe molecules for the investigation of noble metal distribution on porous solids, the following requirements have to be considered: (i) the formation of stable metal-organic complexes, (ii) the molecule size of the probe molecules and the formed complexes should allow distinguishing between metal location inside and outside of pores and cages, (iii) the procedure of sample preparation should be simple for improving the reproducibility, and (iv) the formed metal organic complexes should have characteristic spectroscopic parameters.

In the present work, the formation of metal organic complexes by adsorption of triphenylphosphine (PPh_3) with a molecular diameter of 0.72 nm [16] to noble metal-containing mesoporous and microporous support materials is compared to the one of tris(4-methoxyphenyl) phosphine $P(PhOMe)_3$ having a calculated molecular diameter of 0.91 nm [17,18]. For this purpose, silica A200, mesoporous SBA-15, and two zeolites Y (Si/Al = 93 and 2.7) were loaded with similar amounts of Pt, Rh, Pd, and Ru atoms. The structure of zeolite Y is composed of hexagonal prisms, sodalite cages with an inner diameter of 0.66 nm [19], and supercages with an inner diameter of 1.14 nm [20]. The supercages of zeolite Y are connected via 12-membered oxygen windows with a diameter of 0.74 nm [19]. Considering these structural parameters, PPh_3 is able to enter the 12-ring windows of zeolite Y, while $P(PhOMe)_3$ is too large for entering the 12-ring windows, and, therefore, the supercages of this zeolite. Comparative studies of the formation of metal organic complexes by adsorption of PPh_3 and $P(PhOMe)_3$ on noble metal-containing zeolites Y, therefore, has the potential of clearly distinguishing between noble metals located either *inside* and *outside* of the zeolite particle. In Scheme 1 provides a survey of the most important parameters of the support materials, probe molecules and noble metals used.

2. Experimental part

2.1. Sample preparation

Commercial silica A200 (Evonik, Hanau, Germany) with a specific surface area of 180 m^2/g and mesopore diameters of up to 4.5 nm was used after calcination for 12 h at 823 K in synthetic air. Loading of this silica with platinum was carried out by stirring 5 g of the silica material in 100 mL of demineralized water at 313 K for 2 h and subsequent addition of 1 M aqueous solution of ammonia until the pH-value of the solution reached 10. Then, an aqueous solution with calculated amounts of $[Pt(NH_3)_4]Cl_2\cdot xH_2O$ (ChemPur), $RhCl_3\cdot xH_2O$ (Alfa Aesar), $[Pd(NH_3)_4]Cl_2\cdot xH_2O$ (Sigma-Aldrich), or $RuCl_3\cdot xH_2O$ (Sigma-Aldrich) was added dropwise. The solution was stirred at 313 K for another 18 h. Finally, the resulting solid was collected by filtration, washed with 1.5 L demineralized water, and dried under atmospheric conditions at 353 K for 12 h.

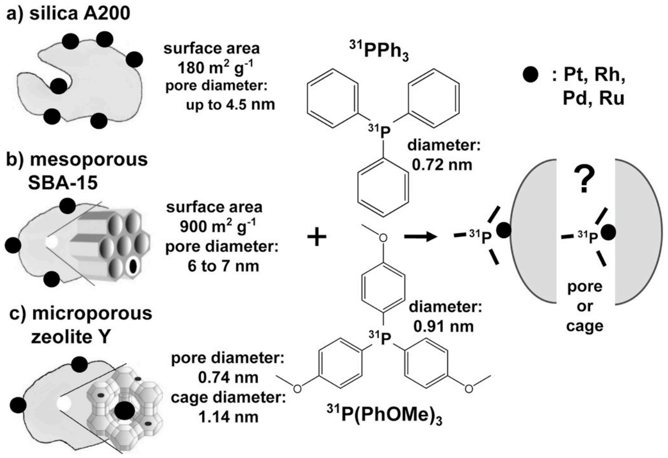

Scheme 1. Survey on the most important parameters of the noble metal (NM) loaded support materials (a to c) and the probe molecules triphenylphosphine, $(PPh)_3$, and tris(4-methoxyphenyl)phosphine, $P(PhOMe)_3$, and schemes of possible NM distributions (left-hand side) as well as possible locations of phosphine complexes formed with NM (right-hand side).

The mesoporous SBA-15 with $n_{Si}/n_{Al} > 1000$, having a specific surface area of 901 m^2/g and mesopore diameters between 6 and 7 nm, was synthesized as described by Zhao et al. [21] The as-synthesized SBA-15 was heated with a rate of 2 K/min up to 823 K and calcined in air for 5 h to remove the template. Subsequently, a wetness impregnation with calculated amounts of the same noble metal salts like for A200 was performed. After stirring the solution for 5 min, the water was removed under vacuum at 313 K and the impregnated materials were dried under atmospheric conditions at 353 K for 12 h.

The dealuminated zeolite DeA-Y with $n_{Si}/n_{Al} = 93$ (Evonik, Hanau, Germany) and zeolite Na–Y with $n_{Si}/n_{Al} = 2.7$ (Evonik, Hanau, Germany) were purified with 1 M aqueous solution of sodium nitrate at 353 K for 4 h and subsequently washed with demineralized water until nitrate-free. The purified zeolites DeA-Y and Na–Y were dried under atmospheric conditions at 353 K for 12 h. The noble metal-containing zeolites derived from DeA-Y were prepared by wetness impregnation using the same procedure as described for the noble metal-containing SBA-15. The noble metal-containing zeolites derived from Na–Y were obtained by aqueous ion exchange with the above-mentioned noble metal salts. For this purpose, purified zeolite Na–Y was suspended in demineralized water containing calculated amounts of these salts at 353 K for 12 h and subsequently washed with demineralized water and dried at 353 K for 24 h.

All noble metal-containing catalysts were calcined in synthetic air (970 mL/min) by heating with a rate of 2 K/min up to 573 K and calcination at this temperature for 3 h, excluding the Ru-containing support materials. The materials were reduced in flowing hydrogen (100 mL/min) at 623 K (Pt-, Rh-, Pd-containing samples) or 673 K (Ru-containing samples) for 2 h, transferred into glass tubes inside a glove box under nitrogen atmosphere, evacuated ($p < 10^{-2}$ Pa) at 298 K for 12 h, and sealed in glass tubes until their use. The total amounts and weight percentages of the noble metal loadings were obtained by optical emission spectroscopy with inductively coupled plasma using a Varian Vista-MPX.

The zeolite H–Y utilized as Brønsted acidic reference material was obtained by a fourfold ion exchange of zeolite Na–Y (side supra) with a 1.0 M aqueous solution of NH_4NO_3 leading to an exchange degree of 91%. Subsequently, this NH_4^+-form zeolite Y was calcined and evacuated ($p < 10^{-2}$ Pa) at 723 K for 12 h to remove ammonia, and sealed in glass tubes.

The microporous silicoalumophosphate VPI-5 utilized as ^{31}P solid-state NMR intensity standard was synthesized as described by He and Klinowski [22]. For spectroscopic studies, this material was utilized in the hydrated state with a water content of 22.0 wt %. The pure support materials were dehydrated and evacuated ($p < 10^{-2}$ Pa) at 723 K for 12 h before the adsorption of probe molecules, while the noble metal-containing support materials were used as obtained after reduction and evacuation at room temperature (vide supra). The adsorption of PPh_3 (Sigma-Aldrich) and $P(PhOMe)_3$ (Sigma-Aldrich) onto the porous materials under study was performed by addition of 4–12 mg of dry PPh_3 or dry $P(PhOMe)_3$ and 40–50 mg of the dehydrated support materials inside a 4 mm rotor. For excluding contact to air, the mixing of probe molecules and support materials was performed in a glove box purged with dry nitrogen. For a proper distribution of the added probe molecules and the formation of metal organic complexes, the rotors were closed with a gas tight TORLON cap and heated at 363 K for 20 h and subsequently equilibrated at room temperature for up to 2 weeks to verify quantitative complex formation.

2.2. *Characterization methods*

The chemical compositions of the noble metal-containing catalysts under study were determined by optical emission spectroscopy (ICP-OES, Varian Vista-MPX). The structural intactness was proven by XRD (Bruker D8 diffractometer) and via ^{27}Al and ^{29}Si solid-state NMR spectroscopy (Bruker AVANCE III 400WB). Specific surface areas and pore volumes were determined by physisorption of nitrogen on an Autosorb-3B (Quantachrome) applying the BET method; results are found in Scheme 1 and in Table S1 in the Supplementary Material (SM). Mesopore volumes were calculated from the total pore volume at $p/p_0 = 0.99$ and the micropore volume according to the V-t method (deBoer). The noble metal dispersion was investigated by chemisorption of hydrogen using the same equipment and assuming a stoichiometry of one H atom per noble metal atom (Autosorb-1, Quantachrome). It was found that Pt, Rh, and Pd are well dispersed, while for Ru-containing samples noble metal dispersions of 40 ± 5% were determined, as expected [23]. The size of P(PhOMe)$_3$ was calculated with the software Avogadro from radii of auto-optimized structures from the PubChem database [17,18] and corrected using a factor calculated from the effective molecular diameter of triphenylphosphine, assuming spherical geometry [16].

^{31}P MAS NMR measurements were carried out on a Bruker Avance III 400WB spectrometer at the resonance frequency of 161.9 MHz using a 4 mm MAS NMR probe with a sample spinning rate of 10 kHz. Spectra were recorded upon $\pi/2$ single-pulse excitation, high-power proton decoupling (HPDEC), and repetition times of 20–240 s for excluding saturation. Quantitative ^{31}P MAS NMR studies were performed by comparing the signal intensities of the samples under study with that of hydrated zeolite VPI-5 used as external intensity standard. The evaluation of the signal intensities was performed as described previously for ^{1}H MAS NMR under additional consideration of different receiver gain values [2].

3. Results and discussion

3.1. *Investigation of PPh$_3$ and P(PhOMe)$_3$ adsorbed on pure support materials*

For investigating the interaction of PPh$_3$ and P(PhOMe)$_3$ with the pure support materials, dehydrated samples of silica A200, mesoporous SBA-15, and zeolites Y were loaded with these probe molecules. The application and procedure of PPh$_3$ as probe molecule in the present study are based on our earlier work [15]. A key aspect of the present investigations is to study the effect of the different sizes of PPh$_3$ and P(PhOMe)$_3$ on the complexation of noble metals on porous support materials (see Scheme 1). For this purpose, PPh$_3$ and P(PhOMe)$_3$ were adsorbed in similar molar quantities on identical samples and thermally treated under the same conditions. Fig. 1 gives a survey on the most important ^{31}P MAS NMR spectra of these phosphine-loaded pure support materials. While bulk PPh$_3$ and P(PhOMe)$_3$ result in narrow signals at $\delta = -9$ and -14 ppm (see Figs. S1a and S1b, SM) [15], physisorption of these molecules on silica A200 and SBA-15 (Fig. 1a–d) is accompanied by low field shifts to $\delta = -6$ and -10 ppm, respectively. This is caused by interactions of the molecules with the siliceous surfaces, either on the exterior or inside the mesopores of A200 and SBA-15.

Physisorption of PPh$_3$ on the siliceous zeolite DeA-Y is accompanied by the occurrence of an additional ^{31}P MAS NMR signal at $\delta = -3$ ppm, which was previously assigned to PPh$_3$ inside the supercages of this zeolite [15]. The ^{31}P MAS NMR spectra of aluminum-containing zeolites Na–Y and H–Y, loaded with PPh$_3$, show signals at $\delta = 1$ and 8 ppm, which are due to PPh$_3$ interacting with Na$^+$ cations and Brønsted acidic bridging OH groups (Si(OH)Al) inside the supercages of zeolite Y, respectively (Fig. 1e–g). Both these signals increase to a maximum with increasing PPh$_3$ loading and additional signals at $\delta = -6$ and -9 ppm, similar to those observed on A200 and SBA-15, occur in the case of a PPh$_3$ surplus.

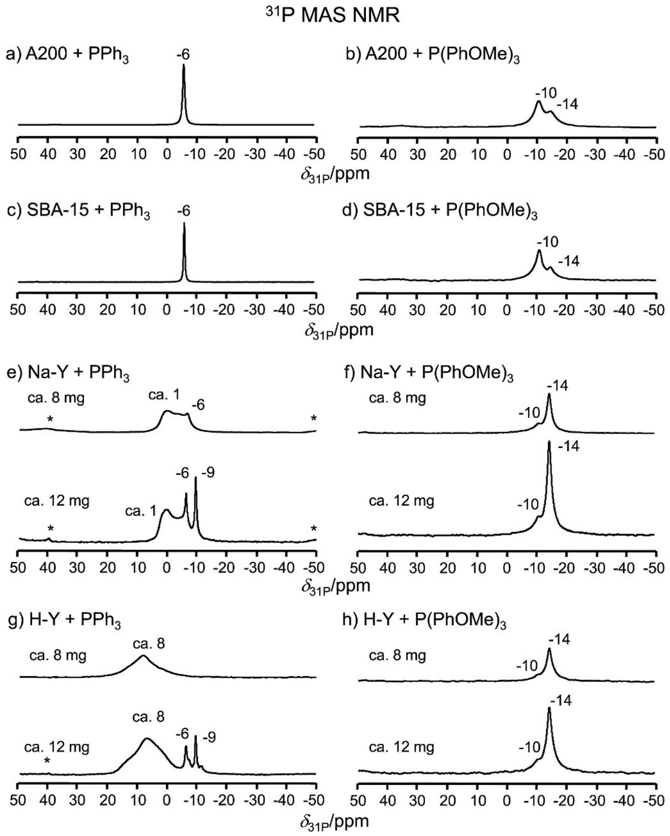

Fig. 1. ^{31}P MAS NMR spectra of PPh$_3$- (left-hand side) and P(PhOMe)$_3$-loaded (right-hand side) pure silica A200 (a, b), mesoporous SBA-15 (c, d), and microporous zeolites Na–Y (e, f) and H–Y (g, h), recorded after heating at 363 K for 20 h and equilibration for up to two weeks at room temperature. Intensities of spectra (a, c) were decreased for clarity. Spinning sidebands are marked by asterisks (*).

Considering the ^{31}P MAS NMR spectra of P(PhOMe)$_3$ loaded on the pure mesoporous and microporous support materials (Fig. 1, right-hand side), exclusively signals of the bulk material at $\delta = -14$ ppm and of physisorbed probe molecules on open surfaces and inside mesopores at $\delta = -10$ ppm can be observed. The different intensity ratios of the signals at $\delta = -14$ and -10 ppm for P(PhOMe)$_3$ loaded on A200 and SBA-15, on the one hand (Fig. 1b–d), and on zeolites Na–Y, and H–Y, on the other hand (Fig. 1f and h), is due to the small external surface of the zeolites Y particles. In contrast, A200 and SBA-15 offer open surface and mesopore surface accessible for P(PhOMe)$_3$, which causes much stronger signals of physisorbed molecules at $\delta = -10$ ppm. The exclusive occurrence of the ^{31}P MAS NMR signals at $\delta = -14$ and -10 ppm for all P(PhOMe)$_3$-loaded pure support materials indicates that this probe molecule cannot enter the 12-ring windows and supercages of zeolites Y. In contrast, PPh$_3$ interacts with Na$^+$ cations (signal at $\delta = 1$ ppm) and Si(OH)Al groups (signal at $\delta = 8$ ppm) inside the supercages, which demonstrates that this molecules is able to enter the 12-membered ring windows of this support material. Hence, two reasons for low field shifts of the ^{31}P MAS NMR signals of the phosphine complexes are present: (i) physisorption on surfaces and (ii) strong steric constraints inside the supercages of zeolites Y. However, the latter exclusively occurs for PPh$_3$ because of the too large size of P(PhOMe)$_3$. A survey on the chemical shift values of PPh$_3$ and P(PhOMe)$_3$ loaded on the support materials under study is given in Table 1.

Table 1
Survey on ^{31}P MAS NMR signals and their assignments to different kinds of PPh_3 (top) and $P(PhOMe)_3$ (bottom) species and phosphine complexes formed with noble metals (NM) on the mesoporous and microporous support materials under study.

δ_{31P}/ppm	Assignment of PPh_3 species
−9	bulk PPh_3
−6	physisorbed PPh_3 on open surfaces and in mesopores
−3	physisorbed PPh_3 in supercages of zeolite Y
ca. 1	PPh_3 coordinated at Na^+ cations in supercages of zeolite Y
8	protonated PPh_3 (PPh_3H^+) in supercages of zeolite Y
ca. 22	decomposed oxidation products of PPh_3
ca. 33	$(PPh_3)_n$NM complexes on open surfaces and in mesopores
ca. 41	$(PPh_3)_n$NM complexes in supercages of zeolite Y
δ_{31P}/ppm	**Assignment of $P(PhOMe)_3$ species**
−14	bulk $P(PhOMe)_3$
−10	physisorbed $P(PhOMe)_3$ on open surfaces and in mesopores
ca. 25	decomposed oxidation products of $P(PhOMe)_3$
ca. 35	$[P(PhOMe)_3]_n$NM complexes on open surfaces and in mesopor

3.2. *Investigation of PPh_3 and $P(PhOMe)_3$ spread on noble metal-containing siliceous support materials*

For the investigation of the complex formation between PPh_3 and $P(PhOMe)_3$, respectively, with Pt, Rh, Pd and Ru, all support materials under study were modified with these noble metals according to the weight percentages given in the sample names in Table 2, column 1, which correspond to the noble metal loadings summarized in Table 2, column 2. As already demonstrated in our previous work [15], on support materials with open surfaces and mesopores, such as silica and SBA-15, respectively, the complexation of PPh_3 with Pt and Rh is accompanied by the occurrence of ^{31}P MAS NMR signals at δ = 30–34 ppm. Similarly, PPh_3 adsorption on Pt-, Rh-, Pd-, and Ru-containing A200 and SBA-15 performed in the present study led to broad low-field ^{31}P MAS NMR signals in this shift range, in addition to narrow signals of bulk and physisorbed PPh_3 at $\delta = -9$ and -6 ppm, respectively. Typical examples are the spectra shown in Fig. 2a and b. After heating the PPh_3/catalyst mixtures at 363 K for 20 h, an equilibration of these samples was performed at room temperature over 1–2 weeks, until no further increase of the ^{31}P MAS NMR signals at ca. 33 ppm could be observed. The quantitative evaluation of these equilibrated low-field signals via comparison with an external intensity standard (VPI-5) led to the numbers of complexed PPh_3 summarized in Table 2, column 3. Considering these experimentally derived numbers of complexed PPh_3 and their corresponding PPh_3/NM ratios (NM = noble metal) in column 4, strong complex formation is found especially for Pt, Rh, and Pd on A200 and SBA-15. This observation hints at a high reactivity of these noble metals and their good accessibility on these support materials for PPh_3. In contrast, significantly lower PPh_3/NM ratios were determined for noble metal-containing zeolites DeA-Y. Small quantities of PPh_3 decomposition products are visible at δ = ca. 25 ppm in Fig. 2e. This hints at a low accessibility of the noble metal species for PPh_3 (molecular diameter of 0.72 nm) due to their location in small sodalite cages (molecular diameter of 0.66 nm) or hexagonal prisms.

Fig. 2 allows the comparison of the ^{31}P MAS NMR spectra of PPh_3 (left-hand side) and $P(PhOMe)_3$ (right-hand side) adsorbed on the same noble metal-containing support materials. For $P(PhOMe)_3$, in addition to broad low-field signals of metal-organic complexes at δ = ca. 35 ppm, narrow signals occur at $\delta = -14$ and -10 ppm, due to excess bulk and physisorbed phosphine molecules, as observed for $P(PhOMe)_3$ adsorbed on pure support materials (Section 3.1.). The evaluation of the intensities of the low-field signals at δ = ca. 35 ppm led to the numbers of complexed $P(PhOMe)_3$ summarized in Table 2, column 5 and the corresponding $P(PhOMe)_3$/NM ratios in Table 2, column 6. The comparison of the PPh_3/NM and $P(PhOMe)_3$/NM ratios in Table 2, columns 4 and 6, respectively, hints at similar reactivities of the different noble metals in the presence of the above-mentioned two phosphines. Partially lower P

Table 2
Noble metal (NM) loadings, numbers of ^{31}P atoms of PPh_3 and $P(PhOMe)_3$ complexed with noble metal (NM) atoms (accuracy ±10%), and corresponding probe molecule to NM ratios.

Samples	NM loading[a] in mmol/g	Complexed PPh_3[b] in mmol/g	PPh_3/NM ratio	Complexed $P(PhOMe)_3$[b] in mmol/g	$P(PhOMe)_3$/NM ratio
1.7 Pt/A200	0.087	0.227	2.6	0.227	2.6
0.9 Rh/A200	0.087	0.216	2.5	0.226	2.3
1.1 Pd/A200	0.103	0.222	2.1	0.089	0.9
1.0 Ru/A200	0.099	0.112	1.2	0.124	1.2
1.9 Pt/SBA-15	0.097	0.281	2.9	0.199	2.0
1.0 Rh/SBA-15	0.097	0.338	3.4	0.186	1.9
1.1 Pd/SBA-15	0.103	0.222	2.3	0.094	0.9
1.2 Ru/SBA-15	0.119	0.204	1.7	0.131	1.1
1.7 Pt/DeA-Y	0.087	0.044	0.5	0.010	0.1
0.9 Rh/DeA-Y	0.087	0.004	0.1	0	0
1.0 Pd/DeA-Y	0.094	0.034	0.4	0	0
0.9 Ru/DeA-Y	0.089	0.027	0.3	0	0

[a] Determined by ICP-OES (accuracy ± 5%).

[b] Determined by ^{31}P MAS NMR spectroscopy (accuracy ±10%).

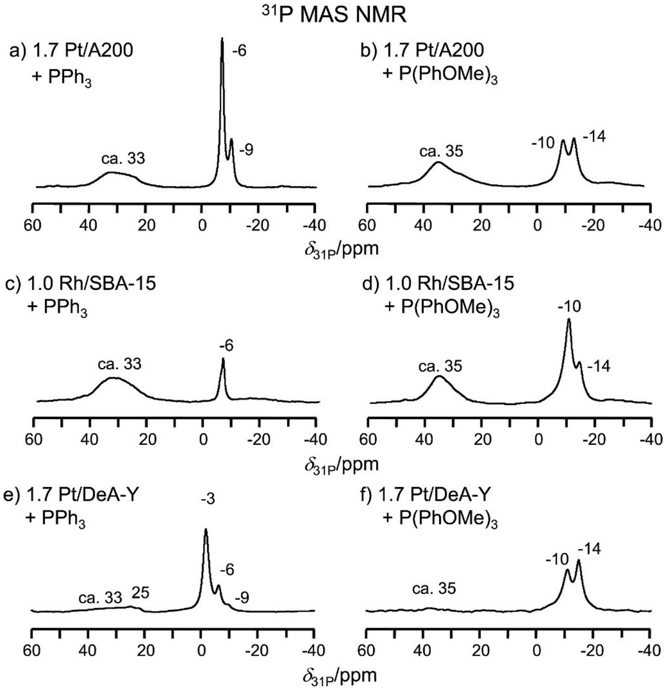

Fig. 2. ^{31}P MAS NMR spectra of PPh_3- (left-hand side) and $P(PhOMe)_3$-loaded (right-hand side) 1.7 Pt/A200 (a, b), mesoporous 1.0 Rh/SBA-15 (c, d), and microporous zeolite 1.7 Pt/DeA-Y (e, f), recorded after heating at 363 K for 20 h and equilibration for up to two weeks at room temperature.

$(PhOMe)_3$/NM than PPh_3/NM ratios for same noble metal-containing support materials are caused by the larger size of $P(PhOMe)_3$ (0.91 nm) compared to PPh_3 (0.72 nm [16]), which leads to increased steric hindrance and less flexibility of the former molecule for less accessible noble metal atoms. Only very weak (1.7 Pt/DeA-Y) or no (other noble metal-containing DeA-Y catalysts) complexation was found for $P(PhOMe)_3$ adsorbed on noble metal-containing zeolite DeA-Y. This observation indicates that minor quantities of the noble metal species on the dealuminated zeolite DeA-Y are located in secondary mesopores, formed as result of the dealumination. These noble metal species are not accessible for the larger $P(PhOMe)_3$, but do react with the smaller PPh_3 (*vide infra*). In the case of siliceous zeolite DeA-Y, the noble metal species were loaded on the support material by wetness impregnation with metal salts. In this case, the noble metal atoms are not guided to well-defined extra-framework cation positions, as in the case of aluminum-rich zeolites Na–Y. In DeA-Y, therefore, noble metal atoms migrate to the most stable positions with strong oxygen coordination, which are inside the small cages, such as sodalite cages and hexagonal prisms of the zeolite Y structure. In these small structural units, noble metal species are not accessible to PPh_3 or $P(PhOMe)_3$. This effect is the reason for the generally lower PPh_3/NM and $P(PhOMe)_3$/NM ratios of noble metal-containing DeA-Y compared with noble metal-containing silica A200 and SBA-15.

3.3. *Investigation of PPh_3 and $P(PhOMe)_3$ spread on noble metal-containing zeolite Na–Y*

The introduction of noble metals on zeolite Na–Y with Si/Al ratio of 2.7 was performed by ion exchange with noble metal salts and subsequent calcination and reduction. In this case, a high content of the noble metal atoms is located at well-defined extra-framework cation positions. In addition to PPh_3 and $P(PhOMe)_3$ adsorption on noble metal-containing DeA-Y, the noble metal guiding properties of the framework aluminum present in zeolite Na–Y have been investigated through the complexation with the above-mentioned phosphines.

The ^{31}P MAS NMR spectra of PPh_3 adsorbed on noble metal-containing zeolite Na–Y in Fig. 3, left-hand side, show the same high-field signals as observed for the pure support material (Fig. 1e), i.e. signals at $\delta = -9$ and -6 ppm for bulk and physisorbed PPh_3, respectively, and a signal at $\delta = 1$ ppm due to PPh_3 adsorbed at Na^+ cations inside the supercages. Weak low-field shoulders on these signals at $\delta =$ ca. 8 ppm hint at the protonation of few of the adsorbed PPh_3 molecules by Brønsted acidic Si(OH)Al groups formed as a result of the noble metal reduction [24,25].

In the low-field range of the spectra in Fig. 3, left-hand side, signals occur between $\delta =$ ca. 33 and 41 ppm for all noble metals (Pt, Rh, Pd, Ru). The former one corresponds to $(PPh_3)_n$NM complexes located without constraints on open surfaces, such as on the external surface of the zeolite particles. For PPh_3 adsorption on pure Na–Y, low-field shifts of ^{31}P MAS NMR signals due to physisorption from $\delta = -9$ to -6 ppm and, upon steric constraints inside of supercages, from $\delta = -9$ to -3 ppm were observed. Therefore, the signal at $\delta = 41$ ppm is assigned to $(PPh_3)_n$NM complexes formed inside the supercages of noble metal-containing zeolites Na–Y. Such $(PPh_3)_n$NM complexes are involved in similar steric constraints as PPh_3 at Na^+cations located in supercages, leading to low-field shifts (vide supra). The total number of complexed PPh_3 on the noble metal-containing zeolites Na–Y under study and the corresponding PPh_3/NM ratios are summarized in Table 3, columns 3 and 4. Decomposition of the low-field signals at $\delta = 33$–41 ppm for the ^{31}P MAS NMR spectra of PPh_3-loaded zeolites 1.9 Pt/Na–Y in Figs. 3a and 0.9 Pd/Na–Y in Fig. 3e showed a contribution of 70 ± 10% of the respective signals at $\delta = 41$ ppm to the total quantity of complexed PPh_3 (see Figs. S2a and 2b in the SM). Thus, for example for 1.9 Pt/Na–Y, this means 0.02 mmol/g of deposited Pt (see Table 3) is located inside the supercages when assuming a stoichiometry of 1:4 [15].

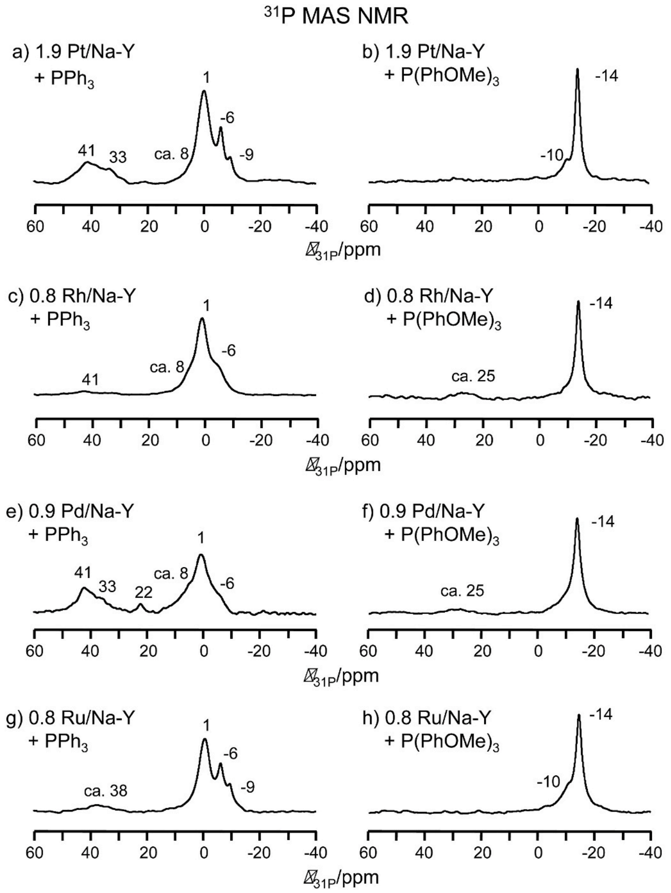

Fig. 3. ^{31}P MAS NMR spectra of PPh_3- (left-hand side) and $P(PhOMe)_3$-loaded (right-hand side) microporous zeolites 1.9 Pt/Na–Y (a, b), 0.8 Rh/Na–Y (c, d), 0.9 Pd/Na–Y (e, f), and 0.8 Ru/Na–Y (g, h), recorded after heating at 363 K for 20 h and equilibration for up to two weeks at room temperature.

Table 3
Noble metal (NM) loadings on Na–Y zeolites, numbers of ^{31}P atoms of PPh_3 and $P(PhOMe)_3$ complexed with noble metal (NM) atoms (accuracy ±10%), and corresponding probe molecules to NM ratios.

Samples	NM loading[a] in mmol/g	Complexed PPh_3[b] in mmol/g	PPh_3 /NM ratio	Complexed $P(PhOMe)_3$[b] in mmol/g	$P(PhOMe)_3$/NM ratio
1.9 Pt/Na–Y	0.097	0.135	1.4	0	0
0.8 Rh/Na–Y	0.078	0.014	0.2	0	0
0.9 Pd/Na–Y	0.085	0.039	0.6	0	0
0.8 Ru/Na–Y	0.079	0.017	0.2	0	0

[a] Determined by ICP-OES (accuracy ± 5%).
[b] Determined by ^{31}P MAS NMR spectroscopy (accuracy ±10%).

According to XRD studies of Gallezot et al. [26], the Pt atoms of zeolites Pt/Na–Y, which were calcined at maximum 573 K, are preferentially located at positions in the supercages, such as at SII in front of the 6-membered ring windows. Also in Pd/Na–Y zeolites, most of the Pd atoms are located at SII positions, while a small content of Pd were found at SI positions inside the hexagonal prisms, due to the slightly smaller size of Pd compared to Pt [27]. These data are in good agreement with the high number of complexed PPh_3 molecules in 1.9 Pt/Na–Y and 0.9 Pd/Na–Y (Table 3, column 4) and the high contents of the signals at $\delta =$ 41 ppm indicating complex formation inside supercages. In contrast, no signal at $\delta = 41$ ppm due to $(PPh_3)_n$NM complexes inside of the supercages could be observed for zeolite 0.8 Ru/Na–Y (Fig. 3g). Also, this finding agrees with the result of XRD studies of comparable materials [28], which localized Ru atoms at SII' positions in front of 6-membered ring windows inside the sodalite cages (diameter of 0.66 nm), i.e. at positions not accessible to PPh_3 (diameter of 0.72 nm). For the noble metal-containing zeolites DeA-Y, generally, a low formation of $(PPh_3)_nNM$ complexes was found (Table 2, lines 1 to 4 from bottom) and no ^{31}P MAS NMR signals occurred at $\delta = 41$ ppm (see, e.g. Fig. 2e). This observation hints at a location of noble metals in siliceous zeolite DeA-Y at well stabilized but non-accessible positions inside sodalite cages and hexagonal prisms due to the absence of the cation- and noble metal-guiding effect of framework aluminum in this material.

Upon adsorption of $P(PhOMe)_3$ on the noble metal-containing zeolites Na–Y, on the other hand, no formation of $[P(PhOMe)_3]_nNM$ complexes could be observed in the ^{31}P MAS NMR spectra in Fig. 3, right-hand side. Signals occurring at ca. $\delta = 25$ ppm are due to the oxidation and decomposition of few of the $P(PhOMe)_3$ molecules, which was also found for PPh_3 on 0.9 Pd/Na–Y, as indicated by the weak signal at $\delta = 22$ ppm. For supportive spectra of triphenylphosphine oxide and $P(PhOMe)_3$ decomposed on pure A200, see Figs. S3a and S3b in the SM. The strong difference in the complex formation upon adsorption of $P(PhOMe)_3$ (0.91 nm) and PPh_3 (0.72 nm) [16] impressively demonstrates that the larger of these molecules is not able to enter the 12-membered ring windows and supercages of zeolites Y. Therefore, $P(PhOMe)_3$ is a very suitable probe molecule for determining noble metals located on the outer surface of zeolite Y particles. PPh_3, on the other hand, can enter the 12-ring windows and supercages of zeolites Y and complexation of this probe molecule inside supercages is accompanied by the occurrence of a characteristic ^{31}P MAS NMR signal at $\delta = 41$ ppm. In the case of complexation of PPh_3 with noble metals outside the supercages of zeolites Y, characteristic signals at $\delta =$ ca. 33 ppm appear. For the dealuminated zeolite DeA-Y, these noble metal atoms could be located in secondary mesopores. For $P(PhOMe)_3$, on the other hand, these noble metal atoms in secondary mesopores are not accessible, since only very weak or no complex formation was found for this probe molecule on noble metal-containing zeolites DeA-Y (see Fig. 3f and Table 2, line 1 to 4 from bottom). For an overview on possible noble metal locations on zeolites DeA-Y and Na–Y and their assignments, complexation with the phosphines under study, and their characteristic ^{31}P MAS NMR signals, see Scheme 2 and Table 4.

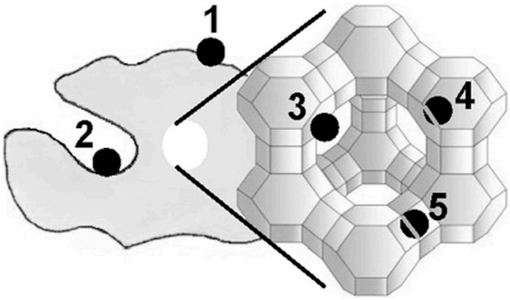

Scheme 2. Possible noble metal (NM) locations on dealuminated zeolite DeA-Y and Al-containing zeolite Na–Y and their assignments according to Table 4.

Table 4
Overview of possible noble metal (NM) locations on dealuminated zeolite DeA-Y and aluminum-containing zeolite Na–Y visualized in Scheme 2, their complex formation with the phosphines under study, and chemical shifts of corresponding ^{31}P MAS NMR signals.

Positions in Scheme 2	Noble metal location	Complexation with phosphines	^{31}P MAS NMR signal (ppm)
1	outer particle surface of DeA-Y and Na–Y	PPh_3 and $P(PhOMe)_3$	ca. 33 and 35
2	secondary mesopores of DeA-Y	PPh_3	ca. 33
3	supercages (SII position) of Na–Y	PPh_3	41
4	sodalite cages (SII′ position)	No	No
5	hexagonal prisms (SI position)	No	No

4. Conclusions

The aim of the present work was the development of methods for the investigation of the spatial location of noble metals (NM) on mesoporous and microporous supports materials, such as silica A200, mesoporous SBA-15, and microporous zeolites Y. For this purpose, two different phosphines (PPh_3, $P(PhOMe)_3$) of different molecular size were used to probe the above-mentioned supports loaded with Pt, Rh, Pd, and Ru. PPh_3 with a molecular diameter of 0.72 nm, is able to enter 12-membered ring windows (diameter of 0.74 nm) and supercages of zeolites Y. On the other hand, an adsorption of $P(PhOMe)_3$ with a molecular diameter of 0.91 nm inside the superages of this zeolite could be excluded. For noble metals on open surfaces of fumed silica (A200) and in mesopores of SBA-15, complexation of PPh_3 as well as of $P(PhOMe)_3$ with all types of noble metals under study was shown by ^{31}P MAS NMR spectroscopy. This complexation of phosphines was found to be accompanied by the occurrence of broad low-field ^{31}P MAS NMR signals at $\delta =$ ca. 33 and 35 ppm, respectively.

In the case of dealuminated zeolite DeA-Y (Si/Al = 93) and zeolite Na–Y (Si/Al = 2.7), different effects of adsorption of PPh_3 and $P(PhOMe)_3$ were observed. For PPh_3, adsorption on noble metal-containing zeolite Na–Y, ^{31}P MAS NMR signals at $\delta = 41$ ppm indicate complex formation inside the supercages of this zeolite. Weak ^{31}P MAS NMR signals at $\delta = 33$–35 ppm observed after PPh_3 as well as $P(PhOMe)_3$ loading hint at the presence of noble metal at the external surface of the zeolite particles. Thus, if the complexation of $P(PhOMe)_3$ on noble metal-containing zeolites Y is much weaker than for PPh_3, location of the noble metal atoms in secondary mesopores, for example, in dealuminated zeolite DeA-Y, must be assumed. Hence, the comparative studies on PPh_3 and $P(PhOMe)_3$ adsorption demonstrated the interesting potential of these probe molecules for quantitatively distinguishing the noble metal distribution on support materials with very different mesoporous and microporous properties.

CRediT authorship contribution statement

C. Rieg: Investigation, Formal analysis, Validation. **D. Dittmann:** Investigation, Validation. **Z. Li:** Investigation. **A. Kurtz:** Investigation. **I. Lorenz:** Investigation. **D.P. Estes:** Conceptualization, Supervision. **M. Buchmeiser:** Conceptualization, Supervision. **M. Dyballa:** Conceptualization, Validation, Project administration, Writing - review & editing. **M. Hunger:** Conceptualization, Validation, Supervision, Writing - original draft.

Declaration of competing interest

The authors declare that they have no known competing financial interests or personal relationships that could have appeared to influence the work reported in this paper.

Acknowledgements

We thank Ann-Katrin Beurer, Marvin Stoll, Dorothea Häussermann, and Heike Fingerle (all University of Stuttgart) for nitrogen adsorption studies and ICP-OES measurements. The authors gratefully acknowledge funding by the Deutsche Forschungsgemeinschaft (DFG, German Research Foundation, project number 358283783 - SFB 1333).

Appendix A. Supplementary data

Supplementary data to this article can be found online at https://doi.org/10.1016/j.micromeso.2020.110594.

References

[1] B. Hu, I.D. Gay, Acid sites on SiO2-Al2O3 monolayer catalysts: 31P NMR probes of strength and accessibility, J. Phys. Chem. B 105 (2001) 217–219.

[2] Y. Jiang, J. Huang, W. Dai, M. Hunger, Solid-state nuclear magnetic resonance investigations of the nature, property, and activity of acid sites on solid catalysts, Solid State Nucl. Magn. Reson. 39 (2011) 116–141.

[3] J.H. Lunsford, W.P. Rothwell, W. Shen, Acid sites in zeolite Y: a solid-state NMR and infrared study using trimethylphosphine as a probe molecule, J. Am. Chem. Soc. 107 (1985) 1540–1547.

[4] Y. Wang, J. Zhuang, G. Yang, D. Zhou, D. Ma, X. Han, X. Bao, Study on the external surface acidity of MCM-22 zeolite: theoretical calculation and 31P MAS NMR, J. Phys. Chem. B 108 (2004) 1386–1391.

[5] A. Zheng, S.-B. Liu, F. Deng, Acidity characterization of heterogeneous catalysts by solid-state NMR spectroscopy using probe molecules, Solid State Nucl. Magn. Reson. 55–56 (2013) 12–27.

[6] R.M. Dessau, Shape-selective platinum/ZSM-5 catalysts, J. Catal. 89 (1984) 520–526.

[7] S. Ernst, Zeolite-entrapped metal complexes, in: G. Ertl, H. Knözinger, F. Schüth, J. Weitkamp (Eds.), Handbook of Heterogeneous Catalysis, Wiley VCH, Weinheim, 2007, pp. 614–631.

[8] J. Weitkamp, S. Ernst, L. Puppe, Shape-selective catalysis in zeolites, in: J. Weitkamp, L. Puppe (Eds.), Catalysis and Zeolites: Fundamentals and Applications, Springer Berlin Heidelberg, Berlin, Heidelberg, 1999, pp. 327–376.

[9] D. Herein, Structure and morphology, in: G. Ertl, H. Knözinger, F. Schüth, J. Weitkamp (Eds.), Handbook of Heterogeneous Catalysis, Wiley VCH, Weinheim, 2007, pp. 765–774.

[10] W.J. Mortier, Compilation of Extra Framework Sites in Zeolites, Butterworth Scientific, Westbury, UK, 1982.

[11] P. Behrens, XANES, EXAFS and related techniques, in: H.G. Karge, J. Weitkamp (Eds.), Characterization I, Springer, Berlin, 2004, pp. 427–466.

[12] D.G. Koningsberger, D.E. Ramaker, Applications of X-ray absorption spectroscopy in heterogeneous catalysis: EXAFS, atomic XAFS and delta XANES, in: G. Ertl, H. Knözinger, F. Schüth, J. Weitkamp (Eds.), Handbook of Heterogeneous Catalysis, Wiley VCH, Weinheim, 2007, pp. 774–803.

[13] U. Obenaus, S. Lang, R. Himmelmann, M. Hunger, Parahydrogen-induced hyperpolarization inside meso- and micropores of Pt-, Rh-, Ir-, and Pd-containing solid catalysts, J. Phys. Chem. C 121 (2017) 9953–9962.

[14] U. Obenaus, F. Neher, M. Scheibe, M. Dyballa, S. Lang, M. Hunger, Relationships between the hydrogenation and dehydrogenation properties of Rh-, Ir-, Pd-, and Pt-containing zeolites Y studied by in situ MAS NMR spectroscopy and conventional heterogeneous catalysis, J. Phys. Chem. C 120 (2016) 2284–2291.

[15] M. Dyballa, C. Rieg, D. Dittmann, Z. Li, M. Buchmeiser, B. Plietker, M. Hunger, Potential of triphenylphosphine as solid-state NMR probe for studying the noble metal distribution on porous supports, Microporous Mesoporous Mater. 293 (2020) 109778.

[16] J. Hjortkjaer, M.S. Scurrell, P. Simonsen, H. Svendsen, Supported liquid phase hydroformylation catalysts containing rhodium and triphenylphosphine. Effects of additional solvents and kinetics, J. Mol. Catal. 12 (1981) 179–195.

[17] National Center for Biotechnology Information, PubChem database. Triphenylphosphine, CID=11776. https://pubchem.ncbi.nlm.nih.gov/compound/Triphenylphosphine. (Accessed 11 May 2020).

[18] National Center for Biotechnology Information, PubChem database. Tris(4-methoxyphenyl)phosphine, CID=70071. https://pubchem.ncbi.nlm.nih.gov/compound/Tris_4-methoxyphenyl_phosphine. (Accessed 11 May 2020).

[19] D.W. Breck, Zeolite Molecular Sieves, Krieger Publishing Company, Malabar, 1975.

[20] J.M. Newsam, The zeolite cage structure, Science 231 (1986) 1093–1099.

[21] D. Zhao, J. Feng, Q. Huo, N. Melosh, G.H. Fredrickson, B.F. Chmelka, G.D. Stucky, Triblock copolymer syntheses of mesoporous silica with periodic 50 to 300 angstrom pores, Science 279 (1998) 548–552.

[22] H. He, J. Klinowski, Synthesis of TBA-VPI-5 and DPA-VPI-5, J. Phys. Chem. 98 (1994) 1192–1197.

[23] R. Oukaci, A. Sayari, J.G. Goodwin, Preparation effects in zeolite-supported metal catalysts: influence of decomposition/reduction on ru particle size, J. Catal. 106 (1987) 318–322.

[24] U. Obenaus, M. Dyballa, S. Lang, M. Scheibe, M. Hunger, Generation and properties of brønsted acid sites in bifunctional Rh-, Ir-, Pd-, and Pt-containing zeolites Y investigated by solid-state NMR spectroscopy, J. Phys. Chem. C 119 (2015) 15254–15262.

[25] D. Santi, S. Rabl, V. Calemma, M. Dyballa, M. Hunger, J. Weitkamp, Effect of noble metals on the strength of brønsted acid sites in bifunctional zeolites, ChemCatChem 5 (2013) 1524–1530.

[26] P. Gallezot, A. Alarcon-Diaz, J.A. Dalmon, A.J. Renouprez, B. Imelik, Location and dispersion of platinum in PtY zeolites, J. Catal. 39 (1975) 334–349.

[27] G. Bergeret, P. Gallezot, B. Imelik, X-ray study of the activation, reduction, and reoxidation of palladium in Y-type zeolites, J. Phys. Chem. 85 (1981) 411–416.

[28] J.R. Pearce, W.J. Mortier, J.B. Uytterhoeven, J.H. Lunsford, Crystallographic study of the distribution of cations in Y-type zeolites containing FeII and FeIII, J. Chem. Soc., Faraday Trans. 1: Physical Chemistry in Condensed Phases 77 (1981) 937–946.